RSC Advances

PAPER

View Article Online
View Journal | View Issue

Cite this: *RSC Adv.*, 2014, **4**, 28432

Molecular dynamics of itraconazole confined in thin supported layers

Emmanuel Urandu Mapesa,*[a] Magdalena Tarnacka,[bc] Ewa Kamińska,[d] Karolina Adrjanowicz,[e] Mateusz Dulski,[bc] Wilhelm Kossack,[a] Martin Tress,[a] Wycliffe Kiprop Kipnusu,[a] Kamil Kamiński[bc] and Friedrich Kremer[a]

Received 21st February 2014
Accepted 17th June 2014

DOI: 10.1039/c4ra01544d

www.rsc.org/advances

Broadband Dielectric Spectroscopy (BDS) is used to study the molecular dynamics of thin layers of itraconazole – an active pharmaceutical ingredient with rod-like structure and whose Differential Scanning Calorimetry (DSC) scans reveal liquid crystalline-like phase transitions. It is found that (i) the structural relaxation process remains bulk like, within the limits of experimental accuracy, in its mean relaxation rate, while (ii) its shape is governed by two competing events: interfacial interactions, and crystalline ordering. Additionally, (iii) the dynamics of the δ-relaxation – assigned to the flip–flop rotation of the molecule about its short axis – deviates from bulk behaviour as the glass transition is approached for the confined material. These observations are rationalized within the framework of molecular dynamics as currently understood.

1 Introduction

To a large extent, the bulk (static and dynamic) properties of low-molecular weight and polymeric materials are well known. In many actual applications (*e.g.* photoresists, batteries, sensors for smart drug delivery, *etc.*) however, the glass formers are confined; they are used in diminished dimensions for purposes of increasing performance and convenience. Consequently, they have – due to an increased surface area to volume ratio – a large fraction of molecules or segments near an interface. How specific aspects of this confinement influence overall properties of the system is a prevailing subject of current soft matter research. To this end, a number of experimental techniques (*e.g.* Ellipsometry,[1,2] X-ray reflectivity,[3] thermal expansion spectroscopy,[4] positron annihilation lifetime spectroscopy,[5] AC-chip Calorimetry,[6] Broadband Dielectric Spectroscopy[2,5,7–10]) have been employed to study key parameters (such as molecular weight,[5,10] tacticity,[11] measurement ambient,[12,13] nature of substrate surface,[2,3,14] concentration of mother solutions[9] and even the type of experiment[15,16]) that may influence dynamics in confinement. While there are contradicting results from various research labs, it is becoming clear that techniques which probe the system in (quasi-equilibrium) liquid state have concurring results, while major variations arise when the system is investigated deep in the (non-equilibrium) glassy state.[16,17]

Thermotropic liquid crystals (LC) are a class of matter with properties intermediate between those of the crystalline and isotropic liquid state. Liquids have maximal mobility and minimal (positional and translational) order while the reverse is true for crystals. In LCs, aspects of both states co-exist, and mesomorphic phases develop with a competing interplay between order and mobility. The most significant liquid crystalline structures are the smectic and nematic mesophases, the latter being the mesophase with the least order. In the nematic regime, molecules have all translational degrees of freedom and hence no long range positional order. Their long axes are favorably aligned with respect to a common unit vector **n**, the so-called nematic director. The degree of orientation[18] of the molecules is described by an order parameter S, given by $S = \langle 3\cos^2\theta - 1\rangle/2$, where θ is the angle between the director **n** and the direction of the long axis of the molecule; the brackets denote statistical averaging. It is easy to see that for a fully aligned LC phase, $S = 1$. The aspect of mobility presents the opportunity to modify the orientations of the molecules by use of external electric (or magnetic) fields. Consequently, broadband dielectric spectroscopy is a versatile tool to study LCs. Liquid crystalline properties arise due to the anisotropy in the shape of the molecules; most of them have a rod-like unit in their structure, although bent-shaped and disc-like units in molecules are also known to give rise to liquid crystalline properties.[19] Since LCs are anisotropic systems, their dielectric

[a]*Institute for Experimental Physics I, University of Leipzig, Linnestr. 5, 04103, Leipzig, Germany. E-mail: urandu@physik.uni-leipzig.de*

[b]*Institute of Physics, University of Silesia, ul. Uniwersytecka 4, 40-007 Katowice, Poland*

[c]*Silesian Center of Education and Interdisciplinary Research, University of Silesia, 75 Pulku Piechoty 1A, 41-500 Chorzów, Poland*

[d]*Department of Pharmacognosy and Phytochemistry, School of Pharmacy and Division of Laboratory Medicine in Sosnowiec, Medical University of Silesia in Katowice, ul. Jagiellonska 4, 41-200 Sosnowiec, Poland*

[e]*NanoBioMedical Centre, Adam Mickiewicz University, Umultowska 85, 61-614 Poznan, Poland*

properties are anisotropic as well, and the complex dielectric function $\varepsilon^*(\omega)$ – where ω is the angular frequency – is given by a tensor. This tensor, in the case of uniaxial nematic phases, has two components $\varepsilon_\parallel{}^*$ and $\varepsilon_\perp{}^*$ parallel and normal, respectively, to the nematic director. For a detailed discussion of the theory of dielectric relaxations in LCs, the reader is referred to other publications.[20–23] Briefly described, the starting point is the fact that the molecular dipole moment vector of a mesogenic unit has two components, one oriented longitudinal and the other transverse to its long axis. The dielectric response arises from correlation functions of the polarization fluctuations parallel and normal to the nematic director. In this semi-microscopic framework, the measured dielectric function parallel $\varepsilon_\parallel{}^*(\omega)$ and normal $\varepsilon_\perp{}^*(\omega)$ to the director has different weighted sums of four underlying relaxation modes depending on the macroscopic orientation of the sample. The relaxation mode with the lowest frequency is due to rotational fluctuations of the molecule around its short axis, and it determines $\varepsilon_\parallel{}^*(\omega)$. This process is called the δ-relaxation.[24–28] The remaining three relaxations – different tumbling fluctuations of the molecules about their long axis – have nearly the same relaxation rate and may form one broad relaxation process, which is related to $\varepsilon_\perp{}^*(\omega)$. This tumbling mode is located at higher frequencies than the δ process. While there has been controversy concerning which of these two processes is responsible for glassy dynamics in glass-forming LCs, recent experiments[26,29] have helped identify the tumbling mode as being the underlying process. A comparison between BDS data in the present work and temperature modulated DSC data published elsewhere[30] (see activation plots) confirms this finding for itraconazole. Therefore the latter process can simply be referred to as the α-process, akin to the structural relaxation process in conventional glass formers.

Itraconazole, the triazole derivative studied in this work, is an active pharmaceutical ingredient (API) with rod-like structure and is known to have antifungal activity.[31] Two relaxation processes[30] have been identified in the bulk material, *i.e.* the structural (α-) relaxation process, and a δ-process (at lower frequencies in the supercooled liquid) whose origin is explained in the foregoing introduction. Additionally, although a first glance at the molecule (Fig. 1a) does not reveal its liquid crystalline-like nature (absence of tail ends), DSC scans find two endothermic peaks that are recognizable as being connected to the formation of nematic and Smectic A phases.[30,32,33] In the current report – using Broadband Dielectric Spectroscopy (BDS) – we follow the dynamics of itraconazole systematically confined in supported layers, down to a thickness of 6 nm.

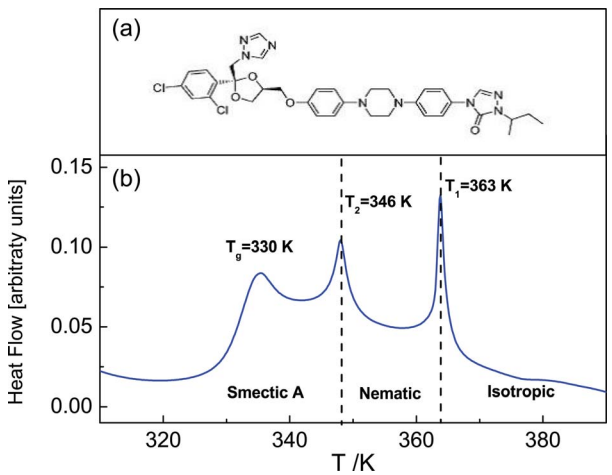

Fig. 1 The chemical structure of the itraconazole molecule (a). A DSC thermogram obtained upon heating of bulk itraconazole – two endothermic transitions associated with liquid crystalline ordering are observed, in addition to the glass transition.

2 Experimental

2.1 Material

The sample material – itraconazole IUPAC name: (2*R*,4*S*)-rel-1-(butan-2-yl)-4-{4-[4-(4-{[(2*R*,4*S*)-2-(2,4-dichlorophenyl)-2-(1*H*-1,2,4-triazol-1-ylmethyl)-1,3-dioxolan-4-yl]methoxy}phenyl)piperazin-1-yl]phenyl}-4,5-dihydro-1*H*-1,2,4-triazol-5-one), molecular formula: $C_{35}H_{38}C_{l2}N_8O_4$, $M_w = 705.64$ g mol^{-1}) was supplied by Sigma Aldrich with purity greater than 99%, and used without further purification. The starting material was completely crystalline with a melting point of 439 K, which agrees with what is reported in the literature (438–451 K).[32] Its chemical structure is displayed in Fig. 1a.

2.2 Methods

2.2.1 Spin-coating. Thin films of itraconazole were prepared by spin-coating from an acetone (Sigma-Aldrich, purity ≥99.9%) solution at a rate of 3000 rpm. Different thicknesses were obtained by varying the concentration of the mother solution: concentrations of 25, 15, 8, 5 and 1 mg ml^{-1} delivered films with thicknesses 123, 83, 46, 22 and 6 nm, respectively. It must be noted here that film thickness was determined, within an uncertainty of ±2 nm, by analyzing (Atomic Force Microscopy) AFM-generated height profiles of scratches made on the films using a sharp stainless steel blade. All solutions were filtered through polytetrafluoroethylene (PTFE) membranes (Merck Millipore) having pores of diameter 200 nm. The films – supported on highly conductive silicon wafers (root-mean-square roughness 0.23 nm measured on a 1 μm^2 scan area, specific resistivity < 3 mΩ cm) with a 30 nm thermally oxidized layer – were then annealed at 380 K for 24 h in an oil-free high vacuum (10^{-6} mbar) before dielectric measurements.

2.2.2 Broadband dielectric spectroscopy (BDS). Nanostructured electrodes[34,35] (see Fig. 2) were used to assemble the capacitors for dielectric measurements. Isobaric measurements of the dielectric permittivity $\varepsilon^*(\omega) = \varepsilon'(\omega) - i\varepsilon''(\omega)$ at ambient pressure were performed using a high-resolution Alpha Analyzer (Novocontrol) over a frequency range from 1 to 3×10^6 Hz. The measured function is denoted in all presentations as ε_{total}'', since it is the total response of the whole active capacitor. It has already been demonstrated that ε_{total}'' still retains the shape and mean relaxation rate of the material under investigation,[36] although the absolute dielectric strength (of the sample) cannot be determined, at least up to now, for this

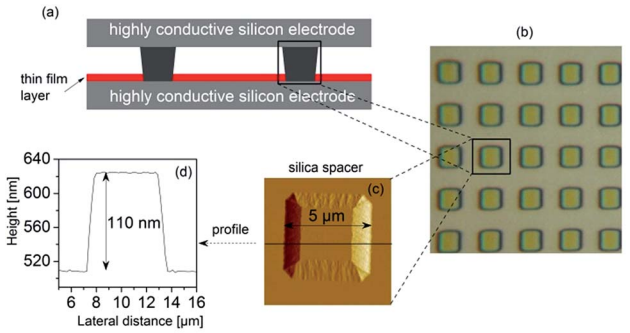

Fig. 2 (a) A scheme of the cross-section of the sample capacitor assembled for dielectric measurements employing ultra-flat highly conductive silicon wafers as electrodes, and insulating silica nano-pillars as spacers; (b) optical microscope image of an array of silica nano-pillars embedded on a conductive silicon wafer; (c) tapping mode AFM height image of a spacer (height 110 nm, lateral dimension 5 µm); and (d) the corresponding profile of the height image.

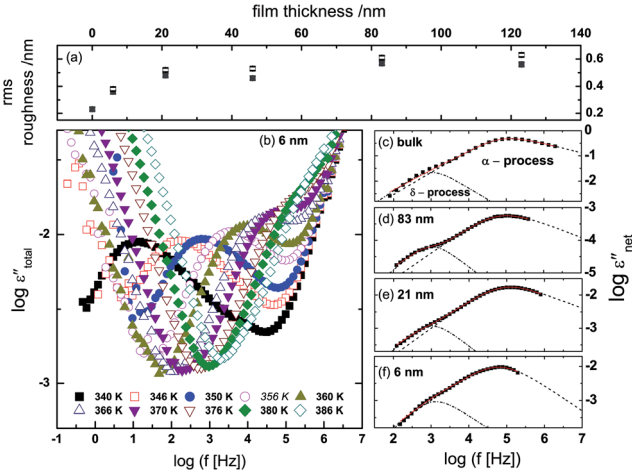

Fig. 3 The root mean square (rms) roughness of the thin film surfaces (determined for a scan area of 1 nm^2) as a function of film thickness, for the as-prepared samples (open squares) and the measured samples (filled squares) (a). Raw dielectric spectra: the imaginary part of the measured permittivity, ε_{total}'', plotted against frequency for a 6 nm-thin itraconazole layer (b). Panels (c), (d), (e) and (f) show the dielectric spectra at 375 K [bulk] and 374 K [thin films] after subtraction of the conductivity contribution and the high-frequency wing; the dashed and dash-dotted lines, respectively, are HN-functions describing the α- and δ-relaxation processes.

specific sample geometry. Temperature control was executed by a Quatro System (Novocontrol) using a jet of dry nitrogen, thereby ensuring relative and absolute errors better than 0.1 and 2 K, respectively. The dielectric measurements were performed in the temperature range 330–386 K after first quenching the samples to the glassy state.

2.2.3 Differential scanning calorimetry (DSC). Thermodynamic properties of crystalline itraconazole were investigated by DSC. Calorimetric measurements were performed using a Mettler-Toledo DSC apparatus equipped with liquid nitrogen cooling accessory and a HSS8 ceramic sensor (heat flux sensor with 120 thermocouples). Temperature and enthalpy calibrations were investigated using indium and zinc standards while heat capacity C_p calibration was performed using a sapphire disc. The crystalline sample was placed in aluminum crucible and heated inside the DSC apparatus and then immediately cooled below the glass transition temperature. Crucibles with such prepared samples were sealed at the top with one puncture, and a scanning rate of 10 K min^{-1} applied over the temperature range 298 to 390 K.

2.2.4 Periodic model calculations. Calculations were performed using the QUANTUM-ESPRESSO (Quantum open-Source Package for Research in Electronic Structure, Simulation, and Optimization – QE) distribution.[37] The Kohn–Sham equations[38] were solved using ultrasoft pseudopotentials.[39,40] Kinetic energy cutoffs were 55 Ry for wave functions and 880 Ry for charge density and potential. Exchange and correlation effects were treated using the local density approximation (LDA) in the form suggested by Perdew and Zunger.[41] Integrations over the Brillouin zone have been performed using the gamma point. The Plane-Wave Self-Consistent Field (PWscf) package was used for optimization of these systems.

3 Results and discussion

The root mean square (rms) roughness of the film surfaces was determined at room temperature by AFM for both the as-prepared and post-measured samples (*i.e.* after annealing and dielectric measurements). It is observed (see Fig. 3a) that (i) there's a tendency for the roughness to increase with layer thickness, but the absolute values remain below 0.7 nm (which is ~10% of the thickness of the thinnest layer prepared) as determined from height images of size 1 nm^2; and (ii) a minimal change in surface roughness (≤8%) is recorded for the post-measured samples when compared to the same sample in the as-prepared state. These findings prove stable film surfaces and exclude effects of dewetting or roughness-induced adulterations of the molecular dynamics.

To analyze the isothermal spectra of the dielectric loss, two Havriliak–Negami (HN) functions[42] were used:

$$\varepsilon''(\omega) = \frac{\sigma_{dc}}{\varepsilon_0 \omega} + \mathrm{Im}\sum_{j=1}^{2}\left\{\varepsilon_\infty + \frac{\Delta\varepsilon_j}{\left[1 + \left(i\omega\tau_j\right)^{\alpha_j}\right]^{\beta_j}}\right\} \quad (1)$$

where the first term accounts for the conductivity contribution, ε_∞ is the permittivity of the unrelaxed medium, α and β are the shape parameters representing the symmetric and asymmetric broadening of the given relaxation peaks, $\Delta\varepsilon$ the dielectric strength, τ the relaxation time, while $\omega = 2\pi f$ is the angular frequency of the applied field.

The measured dielectric response of the thin films in our set up includes some specious conductivity and resistance of the silicon electrodes which cause an increase in the dielectric loss in the low and high frequency flanks, respectively. Fig. 3b is representative data for a 6 nm thin layer, and shows the molecular processes together with the extra contributions on the low and high frequency sides. These spectra show the structural (α-) relaxation process (due to precessing motions of

the molecules), which underlies the dynamic glass transition, and a shoulder between the α-process, and the conductivity contribution. This is a δ-relaxation process – whose genesis is the flip–flop fluctuation of the itraconazole molecule about its short axis – clearly resolved after subtraction of the dc conductivity (see Fig. 3c–f). In Fig. 4, all the dielectric loss spectra (after subtraction of both the conductivity contribution and the high-frequency wing) for bulk itraconazole (panel a) and films of various thickness, *i.e.*, 123, 83, 46, 21 and 6 nm (panels b to f) are presented. As evident from Fig. 3 and 4, the two relaxation processes present in the bulk material are also exhibited by the thin layers.

Fig. 5 shows normalized dielectric loss spectra obtained for all examined samples at 374, 354 and 342 K, that is, temperatures at which, respectively, isotropic, nematic and Smectic A mesophases are expected. In Fig. 6, the evolution of the mean relaxation rate (for the two molecular processes) with temperature, as well as the film-thickness dependence of the dielectrically-determined glass transition temperature, T_g, are presented. It is clearly observed that: (i) at a given temperature (in the nematic and isotropic phases), the structural relaxation peak is broadened (on the lower frequency side) for the thin layers when comparison is made with bulk data (insets-Fig. 5a and b); (ii) there is a tendency (in the Smectic A phase) for the α-peak to narrow down with reducing layer thickness (Fig. 5c); (iii) the mean relaxation rate of the α-process (and hence the dynamic glass transition) remains bulk-like, within the limits of experimental uncertainty, independent of the layer thickness (Fig. 6); (iv) the δ-relaxation exhibits a pronounced slowing down, for the confined molecules, as the LC is cooled towards glass formation (Fig. 6a); and (v) while it is typical of LCs to have

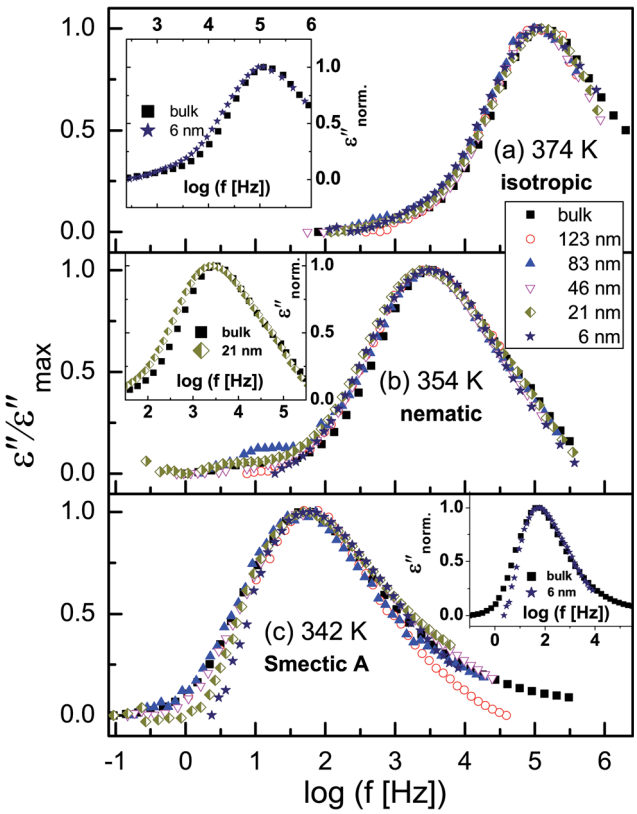

Fig. 5 Dielectric spectra normalized with respect to the maximum of dielectric loss (ε_{max}'') of the α-process at temperatures where the (a) isotropic, (b) nematic and (c) Smectic A mesophases are expected. The insets in (a) and (b) compare data for bulk sample and thin films (thicknesses as indicated) at 374 and 354 K, respectively.

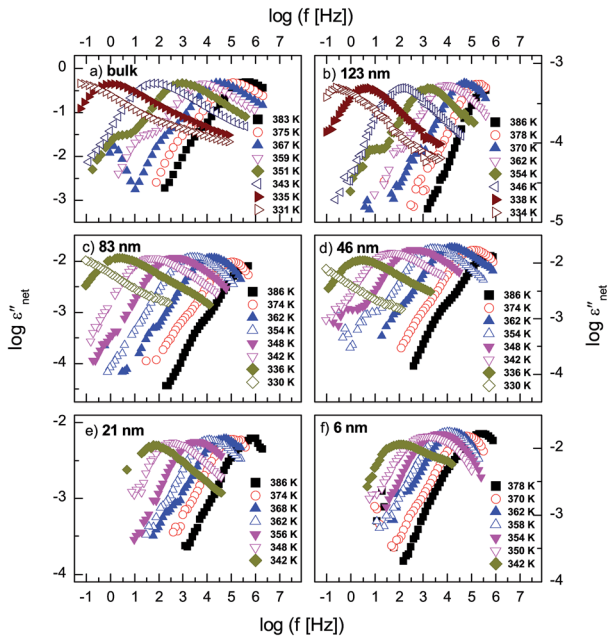

Fig. 4 Dielectric loss, ε_{net}'', (after subtraction of the conductivity contribution and the high-frequency wing) measured above the glass transition temperature for the bulk material [panel a] and films of various thickness as indicated in panels (b) to (f).

just one relaxation process above the clearing temperature,[43] itraconazole has two (Fig. 6a). Each of these observations is rationalized in the following discussion.

Concerning the broadening (at high temperatures) of the structural relaxation process with decreasing thickness, theoretical computations were performed to quantify the interaction between itraconazole and the silica substrate. It is shown (Fig. 7) that hydrogen bonds – with an average length of about 2.05 Å – are formed between oxygen and OH units belonging to, respectively, the carbonyl moiety in itraconazole and silica surface layer. These are relatively strong interactions especially when we keep in mind that, for instance, the average length of the hydrogen bond in water is ~1.96 Å.[44] It has been proven that such attractive interactions lead to immobilization[45] of some of the molecules, hence introducing slower modes (which show up as a broadened peak on the long-time side).[46] Given the immobilization of some molecules in contact with the substrate, it follows that upon heating through the transition, only a fraction of the liquid-crystalline material participates in the disordering. This aspect can aptly be studied by DSC on thin samples, and analyzing the intensity of the transition peaks, but due to technical reasons, this has not yet been realized.

While (attractive) interfacial interactions cause a broadening of the α-peak, crystalline ordering in the sample promotes its

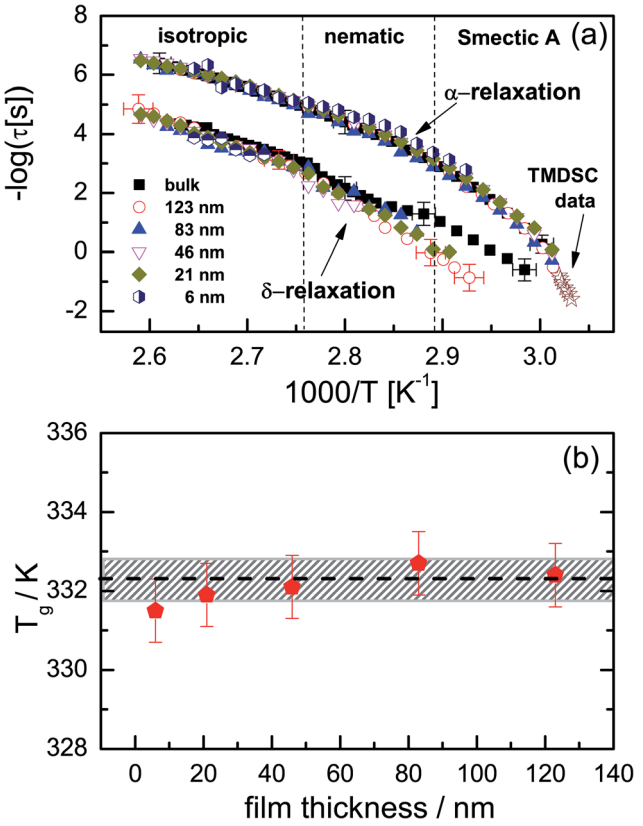

Fig. 6 (a) The temperature-dependence of the mean relaxation times for the α- and δ-processes for different layer thicknesses. The star symbols represent temperature-modulated DSC data (reproduced from ref. 30 with permission from the PCCP Owner Societies) obtained for the bulk sample; (b) the dielectrically-determined glass transition temperature for the layers. The dashed line in (b) represents the calorimetric bulk T_g with its experimental error of ±0.5 K included (shaded region) for completeness.

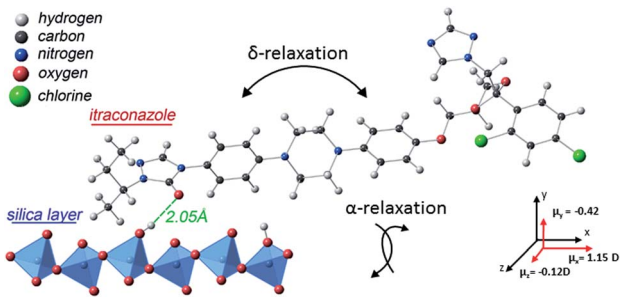

Fig. 7 A visualization of interaction between deposited itraconazole and silica as obtained *via* theoretical computations. The two relaxation processes present in this molecule are also illustrated, together with (calculated) values of the components of the net dipole moment in 3D space.

narrowing. These therefore are competing processes, and whichever one dominates is temperature-determined. At low temperatures, *i.e.*, in the Smectic A phase, the peak tends to narrow down with reducing layer thickness. To understand this, it must be noted that smectic layering begins at the interface,[47] and progresses through the film expanse in the direction perpendicular to the wall; the extent to which smectic ordering permeates the sample volume is therefore inversely proportional to the film thickness. Hence, the thinner the film, the more the order parameter aligns in the direction of the applied electric field.

For the structural relaxation, the temperature-dependence of the mean relaxation times plotted in Fig. 6a were fitted by the Vogel–Fulcher–Tammann (VFT) equation[48–50] which reads

$$\tau(T) = \tau_\infty \exp\{(D_T T_0)/(T - T_0)\}, \quad (2)$$

where the parameters τ, D_T and T_0 are the characteristic relaxation time, the (quantitative measure of) fragility, and the so-called Vogel temperature, respectively. All fitting parameters are collected in Table 1. It is clear that the temperature evolution of the mean structural relaxation times in all investigated samples is the same, within the margins of uncertainty. From the VFT fits (not displayed), the glass transition temperature, T_g, for each sample was evaluated by defining T_g as the temperature at which structural relaxation time is equal to 100 s. The results are presented in Fig. 6b where it is manifest that the glass transition temperature of all the studied film samples remains within a margin of ±2 K of the bulk value. These findings point to the fact that the extent of confinement reached in these experiments is not restrictive enough to change the dynamic glass transition of itraconazole. The question here is: what is the length scale that underlies the (dynamic) glass transition? Kremer *et al.*[51] have experimentally demonstrated that six molecules (for ethylene glycol) are already sufficient to perform bulk-like dynamics (in terms of the mean relaxation rate), and that such dynamics persist to a length scale as small as 1.5 nm for propylene glycol. This is consistent with experimental,[52–55] theoretical[56] as well as computational[53] investigations of larger molecules where the length of the basic fluctuating unit has been estimated to be just about a nanometer.

The flip–flop fluctuation of the molecule about its short axis (δ-relaxation) is, naturally, a slow process because of its coupling to the centres of mass.[57] Given this fact, it follows that geometrically induced restrictions should further slowdown the movement, especially at low temperatures. Since the data in Fig. 6 does not reveal a thickness-dependence of the slowing down, we infer that the main cause of this phenomenon is the spin casting process itself. A number of studies have shown that the spin-coating procedure introduces conformational changes[58,59] which have a direct consequence on the ensuing molecular dynamics.[9,60–62]

Table 1 VFT parameters of the α-relaxation process for the studied samples, and the respective T_g values obtained as discussed in the text

Sample	log τ	D_T	T_0	$T_g \pm 1$ K
Bulk	−9.8 ± 0.1	635.8 ± 27.3	305.2 ± 0.7	332.5
123 nm	−10.4 ± 0.2	777.9 ± 49.2	300.5 ± 1.8	332.4
83 nm	−11.1 ± 0.2	972.0 ± 48.4	294.6 ± 1.3	332.7
46 nm	−10.2 ± 0.1	729.6 ± 23.9	301.1 ± 0.7	332.1
21 nm	−10.5 ± 0.1	801 ± 17	298.3 ± 0.5	331.9
6 nm	−10 ± 1	684.6 ± 296.1	299.8 ± 10.5	331.5

Finally, we turn our attention to the presence of two relaxation processes above the clearing temperature. Typically, only one relaxation process is expected in the isotropic mesophase because the liquid state dominates. The two processes registered in (bulk and confined) itraconazole, however, suggest that the molecules can still undergo distinguishable motions about their short and long axes, as would be the case in the more-ordered phases. Theoretical predictions,[63] and some X-ray diffraction (XRD) experiments have hinted at the existence of nematic clusters[64–67] which may not disappear[68] even at high temperatures in some LCs. Consequently, local, randomly oriented nematic-ordered structures (clusters) – without long-range ordering – can be found in the isotropic liquid phase. Our dielectric results therefore provide proof of the existence of a locally ordered phase in the temperature regime where isotropism would be expected to prevail.

4 Conclusions

In this paper, the molecular dynamics of confined itraconazole were investigated and compared to the bulk material. It is shown that the mean structural relaxation times – and hence the dynamic glass transition – remain bulk-like in the accessible temperature range even for the thinnest studied sample of 6 nm. The distribution of these relaxation times is affected by two competing events: the interfacial interactions and crystalline ordering in the sample. It is also demonstrated that confinement of itraconazole in thin layers slows down the molecules' flip–flop motion (about their short axes) as the glass transition is approached from the upper side. These results provide further understanding of liquid crystal behaviour in confinement, and bear direct consequences to their applicability in nanotechnology.

Acknowledgements

E.U.M and F.K are grateful for funding received from the German Research Foundation, respectively, within the Focused Research Program SPP 1369, and in the framework of the Centre for Collaborative Research (SFB-TRR 102) of the Universities of Martin-Luther (Halle-Wittenberg) and Leipzig. M.T.[a] appreciates financial support from the Graduate School BuildMoNa. Financial support from the Polish National Science Centre, decisions DEC-2013/09/D/NZ7/04194 and DEC-2012/05/B/ST4/00089, for E.K. and M.T.[b], and K.K., respectively, is ackowledged. K.A. thanks the National Centre for Research and Development (nanomaterials and their potential application in nanobiomedicine) for grants. This research was also financed by the Medical University of Silesia as part of Research for Young Scientists (Contract No. KNW-2-004/N/4/N). Support from the PL-Grid Infrastructure is also appreciated. We thank Gladys Mumbua for fruitful discussions.

References

1 J. L. Keddie, R. A. L. Jones and R. A. Cory, *Europhys. Lett.*, 1994, **27**, 59–64.
2 M. Erber, M. Tress, E. U. Mapesa, A. Serghei, K.-J. Eichhorn, B. Voit and F. Kremer, *Macromolecules*, 2010, **43**, 7729–7733.
3 G. Reiter, *Macromolecules*, 1994, **27**, 3046–3052.
4 K. Fukao and Y. Miyamoto, *Phys. Rev. E: Stat., Nonlinear, Soft Matter Phys.*, 2001, **64**, 011803.
5 G. B. DeMaggio, W. E. Frieze, D. W. Gidley, M. Zhu, H. A. Hristov and A. F. Yee, *Phys. Rev. Lett.*, 1997, **78**, 1524–1527.
6 H. Huth, A. A. Minakov and C. Schick, *J. Polym. Sci., Part B: Polym. Phys.*, 2006, **44**, 2996–3005.
7 F. Kremer, A. Serghei, J. R. Sangoro, M. Tress and E. U. Mapesa, *IEEE Trans. Dielectr. Electr. Insul.*, 2009, DOI: 10.1109/CEIDP.2009.5377717.
8 E. U. Mapesa, M. Erber, M. Tress, K.-J. Eichhorn, A. Serghei, B. Voit and F. Kremer, *Eur. Phys. J.: Spec. Top.*, 2010, **189**, 173–180.
9 E. U. Mapesa, M. Tress, G. Schulz, H. Huth, C. Schick, M. Reiche and F. Kremer, *Soft Matter*, 2013, **9**, 10592–10598.
10 M. Tress, M. Erber, E. U. Mapesa, H. Huth, J. Müller, A. Serghei, C. Schick, K.-J. Eichhorn, B. Voit and F. Kremer, *Macromolecules*, 2010, **43**, 9937–9944.
11 Y. Grohens, L. Hamon, G. Reiter, A. Soldera and Y. Holl, *Eur. Phys. J. E: Soft Matter Biol. Phys.*, 2002, **8**, 217–224.
12 A. Serghei, H. Huth, M. Schellenberger, C. Schick and F. Kremer, *Phys. Rev. E: Stat., Nonlinear, Soft Matter Phys.*, 2005, **71**, 061801.
13 A. N. Raegen, M. V. Massa, J. A. Forrest and K. Dalnoki-Veress, *Eur. Phys. J. E: Soft Matter Biol. Phys.*, 2008, **27**, 375–377.
14 J. A. Forrest, K. Dalnoki-Veress, J. R. Stevens and J. R. Dutcher, *Phys. Rev. Lett.*, 1996, **77**, 2002–2005.
15 O. Bäumchen, J. D. McGraw, J. A. Forrest and K. Dalnoki-Veress, *Phys. Rev. Lett.*, 2012, **109**, 055701.
16 V. M. Boucher, D. Cangialosi, H. Yin, A. Schönhals, A. Alegría and J. Colmenero, *Soft Matter*, 2012, **8**, 5119–5122.
17 F. Kremer, E. U. Mapesa, M. Tress, and M. Reiche, in *Recent Advances in Broadband Dielectric Spectroscopy*, ed. Y. P. Kalmykov, Springer, Dordrecht, 2011, pp. 163–178.
18 S. Chandrasekhar, *Liquid Crystals*, Cambridge University Press, Cambridge, 2nd edn, 1992.
19 *Handbook of liquid crystals*, ed. D. Demus, J. Goodby, G. W. Gray, H. W. Spiess and V. Vill, Wiley-VCH, Weinheim, 1998.
20 P. Luigi Nordio, G. Rigatti and U. Segre, *Mol. Phys.*, 1973, **25**, 129–136.
21 G. S. Attard, K. Araki and G. Williams, *Br. Polym. J.*, 1987, **19**, 119–127.
22 K. Araki, G. S. Attard, A. Kozak, G. Williams, G. W. Gray, D. Lacey and G. Nestor, *J. Chem. Soc., Faraday Trans. 2*, 1988, **84**, 1067–1081.
23 *Broadband Dielectric Spectroscopy*, ed. F. Kremer and A. Schönhals, Springer-Verlag, Berlin, 2003.
24 W. H. de Jeu, *Physical properties of liquid crystalline material*, Gordon & Breach, New York, London, Paris, 1979.
25 C. Baehr, B. Glüsen, J. H. Wendorff and E. G. Staring, *Macromol. Rapid Commun.*, 1994, **15**, 327–333.
26 A. Brás, M. Dionísio, H. Huth, C. Schick and A. Schönhals, *Phys. Rev. E: Stat., Nonlinear, Soft Matter Phys.*, 2007, **75**, 061708.

27 A. R. Brás, S. Frunza, L. Guerreiro, I. M. Fonseca, A. Corma, L. Frunza, M. Dionísio and A. Schönhals, *J. Chem. Phys.*, 2010, **132**, 224508.
28 C. Grigoriadis, H. Duran, M. Steinhart, M. Kappl, H.-J. Butt and G. Floudas, *ACS Nano*, 2011, **5**, 9208–9215.
29 C. Schick, D. Sukhorukov and A. Schönhals, *Macromol. Chem. Phys.*, 2001, **202**, 1398–1404.
30 M. Tarnacka, K. Adrjanowicz, E. Kaminska, K. Kaminski, K. Grzybowska, K. Kolodziejczyk, P. Wlodarczyk, L. Hawelek, G. Garbacz, A. Kocot and M. Paluch, *Phys. Chem. Chem. Phys.*, 2013, **15**, 20742.
31 J. Van Cutsem, F. Van Gerven, M. A. Van de Ven, M. Borgers and P. A. Janssen, *Antimicrob. Agents Chemother.*, 1984, **26**, 527–534.
32 K. Six, G. Verreck, J. Peeters, K. Binnemans, H. Berghmans, P. Augustijns, R. Kinget and G. Van den Mooter, *Thermochim. Acta*, 2001, **376**, 175–181.
33 K. Six, G. Verreck, J. Peeters, P. Augustijns, R. Kinget and G. Van den Mooter, *Int. J. Pharm.*, 2001, **213**, 163–173.
34 A. Serghei and F. Kremer, *Rev. Sci. Instrum.*, 2008, **79**, 026101.
35 F. Kremer, M. Tress and E. U. Mapesa, *Dielectrics Newsletter*, 2012, **10**, 1–3.
36 A. Serghei, M. Tress and F. Kremer, *J. Chem. Phys.*, 2009, **131**, 154904.
37 P. Giannozzi, S. Baroni, N. Bonini, M. Calandra, R. Car, C. Cavazzoni, D. Ceresoli, G. L. Chiarotti, M. Cococcioni, I. Dabo, A. Dal Corso, S. de Gironcoli, S. Fabris, G. Fratesi, R. Gebauer, U. Gerstmann, C. Gougoussis, A. Kokalj, M. Lazzeri, L. Martin-Samos, N. Marzari, F. Mauri, R. Mazzarello, S. Paolini, A. Pasquarello, L. Paulatto, C. Sbraccia, S. Scandolo, G. Sclauzero, A. P. Seitsonen, A. Smogunov, P. Umari and R. M. Wentzcovitch, *J. Phys.: Condens. Matter*, 2009, **21**, 395502.
38 W. Kohn and L. J. Sham, *Phys. Rev.*, 1965, **140**, A1133–A1138.
39 M. C. Payne, M. P. Teter, D. C. Allan, T. A. Arias and J. D. Joannopoulos, *Rev. Mod. Phys.*, 1992, **64**, 1045–1097.
40 D. Vanderbilt, *Phys. Rev. B: Condens. Matter Mater. Phys.*, 1990, **41**, 7892.
41 J. P. Perdew and A. Zunger, *Phys. Rev. B: Condens. Matter Mater. Phys.*, 1981, **23**, 5048.
42 S. Havriliak and S. Negami, *Polymer*, 1967, **8**, 161–210.
43 M. Davies, R. Moutran, A. H. Price, M. S. Beevers and G. Williams, *J. Chem. Soc., Faraday Trans. 2*, 1976, **72**, 1447–1458.
44 A. C. Legon and D. J. Millen, *Chem. Soc. Rev.*, 1987, **16**, 467–498.
45 S. Napolitano and M. Wübbenhorst, *Nat. Commun.*, 2011, **2**, 260–267.
46 M. Tress, E. U. Mapesa, W. Kossack, W. K. Kipnusu, M. Reiche and F. Kremer, *Science*, 2013, **341**, 1371–1374.
47 J. T. Mang, K. Sakamoto and S. Kumar, *Mol. Cryst. Liq. Cryst.*, 1992, **223**, 133–142.
48 H. Vogel, *Phys. Z.*, 1921, **22**, 645–646.
49 G. S. Fulcher, *J. Am. Ceram. Soc.*, 1925, **8**, 339–355.
50 G. Tammann and G. Hesse, *Z. Anorg. Allg. Chem.*, 1926, **156**, 245–257.
51 F. Kremer, A. Huwe, M. Arndt, P. Behrens and W. Schwieger, *J. Phys.: Condens. Matter*, 1999, **11**, A175–A188.
52 I. Bahar, B. Erman, F. Kremer and E. W. Fischer, *Macromolecules*, 1992, **25**, 816–825.
53 E. Donth, H. Huth and M. Beiner, *J. Phys.: Condens. Matter*, 2001, **13**, L451–L462.
54 A. Schönhals, H. Goering, C. Schick, B. Frick and R. Zorn, *Colloid Polym. Sci.*, 2004, **282**, 882–891.
55 L. Berthier, *Science*, 2005, **310**, 1797–1800.
56 E.-J. Donth, *J. Non-Cryst. Solids*, 1982, **53**, 325–330.
57 C. M. Roland, *Soft Matter*, 2008, **4**, 2316.
58 A. Brûlet, F. Boué, A. Menelle and J. P. Cotton, *Macromolecules*, 2000, **33**, 997–1001.
59 H. Tsuruta, Y. Fujii, N. Kai, H. Kataoka, T. Ishizone, M. Doi, H. Morita and K. Tanaka, *Macromolecules*, 2012, **45**, 4643–4649.
60 A. Serghei and F. Kremer, *Phys. Rev. Lett.*, 2003, **91**, 165702.
61 A. Serghei, F. Kremer and W. Kob, *Eur. Phys. J. E: Soft Matter Biol. Phys.*, 2003, **12**, 143–146.
62 M. Solar, E. U. Mapesa, F. Kremer, K. Binder and W. Paul, *EPL*, 2013, **104**, 66004.
63 L. V. Azároff, *Proc. Natl. Acad. Sci. U. S. A.*, 1980, **77**, 1252–1254.
64 I. G. Chistyakov and W. M. Chaikowsky, *Mol. Cryst.*, 1969, **7**, 269–277.
65 A. D. Vries, *Mol. Cryst. Liq. Cryst.*, 1970, **10**, 31–35.
66 O. Francescangeli and E. T. Samulski, *Soft Matter*, 2010, **6**, 2413.
67 C. Keith, A. Lehmann, U. Baumeister, M. Prehm and C. Tschierske, *Soft Matter*, 2010, **6**, 1704.
68 A. D. Vries, *Mol. Cryst. Liq. Cryst.*, 1970, **10**, 219–236.